Monthly Notices of the ROYAL ASTRONOMICAL SOCIETY
MNRAS **455,** 1782–1795 (2016) doi:10.1093/mnras/stv2366

Giant molecular cloud scaling relations: the role of the cloud definition

S. A. Khoperskov,[1,2,3★] E. O. Vasiliev,[4,5] D. A. Ladeyschikov,[6] A. M. Sobolev[6] and A. V. Khoperskov[7]

[1]*Dipartimento di Fisica, Università degli Studi di Milano, via Celoria 16, I-20133 Milano, Italy*
[2]*Institute of Astronomy, Russian Academy of Sciences, Pyatnitskaya st. 48, 119017 Moscow, Russia*
[3]*Sternberg Astronomical Institute, Moscow M.V. Lomonosov State University, Universitetskij pr. 13, 119992 Moscow, Russia*
[4]*Institute of Physics, Department of Physics, Southern Federal University, Sorge 5, Rostov on Don 344090, Russia*
[5]*Special Astrophysical Observatory, RAS, Nizhnii Arkhyz, Karachaevo-Cherkesskaya Republic, 369167 Russia*
[6]*Ural Federal University, 51 Lenin Str., Ekaterinburg 620000, Russia*
[7]*Volgograd State University, Universitetsky pr. 100, 400062 Volgograd, Russia*

Accepted 2015 October 9. Received 2015 October 8; in original form 2015 March 2

ABSTRACT

We investigate the physical properties of molecular clouds in disc galaxies with different morphologies: a galaxy without prominent structure, a spiral barred galaxy and a galaxy with flocculent structure. Our *N*-body/hydrodynamical simulations take into account non-equilibrium H_2 and CO chemical kinetics, self-gravity, star formation and feedback processes. For the simulated galaxies, the scaling relations of giant molecular clouds, or so-called Larson's relations, are studied for two types of cloud definition (or extraction method): the first is based on total column density position–position (PP) data sets and the second is indicated by the CO (1–0) line emission used in position–position–velocity (PPV) data. We find that the cloud populations obtained using both cloud extraction methods generally have similar physical parameters, except that for the CO data the mass spectrum of clouds has a tail with low-mass objects $M \sim 10^3$–10^4 $M_\odot$. Owing toa varying column density threshold, the power-law indices in the scaling relations are significantly changed. In contrast, the relations are invariant to the CO brightness temperature threshold. Finally, we find that the mass spectra of clouds for PPV data are almost insensitive to the galactic morphology, whereas the spectra for PP data demonstrate significant variation.

Key words: ISM: clouds – ISM: molecules – ISM: structure – stars: formation – galaxies: spiral – galaxies: structure.

1 INTRODUCTION

Molecular gas in galaxies is mostly concentrated in cold clouds with masses $\simeq 10^{4-5}$ $M_\odot$, which are usually called giant molecular clouds (GMCs). Their evolution is important for understanding the transition of the gaseous component into the stellar one. Indeed, galactic star formation generally occurs in the dense medium of GMCs. Larson (1981) initially introduced three empirical scaling relations for nearby molecular clouds in the Milky Way (MW). These relations reflect the general view of GMC properties and have the following sense.

(i) The cloud size–line-of-sight velocity dispersion relation, $\sigma_v \propto R^{\beta_1}$, is the first; it argues that the cloud structure is supported by internal turbulence.

(ii) The cloud virial mass–luminosity in CO lines relation, $M_{vir} \propto L_{CO}^{\beta_2}$, is the second; it shows that GMCs are structures in virial equilibrium.

(iii) The luminosity in CO lines (sometimes the cloud mass used)–size, $L_{CO} \propto R^{\beta_3}$, is the third; it implies that the mean cloud surface density Σ_0 is likely to be constant if $\beta_3 \approx 2$.

Despite long study of the scaling relations, a complete theoretical explanation for the origin of the relations has not been offered yet. Based on CO observations of molecular clouds in the Galactic disc, it has been found that GMCs have approximately constant surface density $\sim$170 $M_\odot$ pc^{-2} and the state of the clouds is very close to virial equilibrium (Solomon et al. 1987). Roman-Duval et al. (2010) have found a tight power-law correlation with index 2.36 ± 0.04 between the radii and masses of Galactic molecular clouds. The virial parameter of the derived clouds is mostly below 1 with a mean value of 0.46, so that clouds are strongly self-gravitating. Using ^{12}CO data, Heyer et al. (2009) re-examined the scaling relations for Galactic clouds under the assumption of constant CO-to-H_2

★ E-mail: sergey.khoperskov@unimi.it

conversion factor within a cloud. This leads to a lower median mass surface value, which is 42 $M_\odot$ pc^{-2}. Note that the clouds found in this study are mostly unbound, which is in contradiction to previous studies. Thus, the observational data demonstrate significant scatter in the physical state of GMCs even in the MW.

For molecular clouds in both dwarf and giant disc galaxies, Bolatto et al. (2008) have found scaling relations similar to those for MW clouds. They have concluded that GMCs identified on the basis of their CO emission constitute a unique class of objects, exhibiting a remarkably uniform set of properties from galaxy to galaxy. Meanwhile, more recent comparison of GMCs in nearby galaxies by Hughes et al. (2013) has allowed us to figure out that GMC properties (mass, radius, velocity dispersion) are not robust towards external conditions: clouds are smaller and fainter in less dense regions, i.e. inside low-mass galaxies and in the outer regions of the Galaxy, compared with molecular structures in denser environments, e.g. in the inner part of the Galaxy and other spirals like M51 (Colombo et al. 2014) and M33 (Engargiola et al. 2003; Bigiel et al. 2010).

Certainly, the scaling relations can reflect some universality in both physical conditions inside clouds and the interaction of clouds with the ambient medium. GMC properties and evolution are governed by the interplay between self-gravity, magnetic field and feedback processes from stars born inside clouds. In many theoretical studies, there have been attempts to understand how various feedback processes influence the properties of GMCs (Shetty & Ostriker 2008; Tasker 2011; Hopkins, Quataert & Murray 2012; Braun et al. 2014). For instance, Dobbs, Burkert & Pringle (2011) have traced the evolution of individual clouds in detail and found that cloud–cloud collisions and stellar feedback can regulate internal velocity dispersion and lead to the formation of unbound GMCs. Contrary to the previous study, Tasker & Tan (2009) suggested that molecular clouds are gravitationally bound because of the low collisional rate of clouds relative to the orbital time-scale. Thus, internal turbulent energy can keep molecular clouds in virial equilibrium. Several simulations of turbulence in GMCs (Renaud et al. 2013; Kritsuk, Lee & Norman 2013) have justified the idea that self-gravity plays an important role in the cloud structure, but does not affect the 'velocity dispersion–size' relation strongly.

Using high-resolution simulations, Benincasa et al. (2013) analysed the physical properties of clouds with number density above 100 cm^{-3}. They found that the slopes of the 'velocity dispersion–size' and 'mass–size' relations appear to be much steeper than the observational ones. On the other hand, Tasker & Tan (2009) obtained good agreement between the mass, radius and velocity dispersion of GMCs and those observed in the Galaxy. Such contradictory conclusions are explained by not only differences in simulations, e.g. taking into account star formation and other processes, but also the variety in samples of clouds caused by using different methods of cloud extraction. Moreover, Fujimoto et al. (2014) found a significant effect of the galactic environment on the cloud properties in a dynamical model of M83. At first they established that the 'mass–size' relation has a bimodal distribution and, secondly, GMCs tend to be less gravitationally bound in denser environments, i.e. spiral arms or a bar, than in rarefied ones, e.g. inside a disc.

In numerical simulations, a cloud is usually defined as an object with gas density (column or volume) higher than a given threshold. Such an object can consist of several dense molecular cloudlets surrounded by diffuse intercloud molecular and/or atomic gas. In addition, there are several other methods for cloud definition based on dust extinction, molecular or/and atomic column density or CO intensity. For each method, it is interesting to find the scaling relation and compare it with the empirical one established by Larson. This allows us to understand better what interstellar medium (ISM) structures are responsible for the appearance of these relations.

The matching of the observed and simulated GMC properties is not obvious, because of the different approaches used for cloud definition. In general, this problem has no unique solution in observations, because in observations the border of a cloud can depend on a chosen signal-to-noise limit. In numerical simulations, there are two commonly used methods for cloud extraction. The first one is based on total column density position–position (henceforth PP) data sets and the second is indicated by the CO line emission using position–position–velocity (PPV) data. The latter is utilized in the CLUMPFIND (Williams, de Geus & Blitz 1994) and CPROPS (Rosolowsky & Leroy 2006) packages.

In this article, we consider the physical properties (namely mass, radius, surface density, velocity dispersion, luminosity, etc.) of clouds for two methods of cloud extraction based on PP and PPV data sets. In our simulations, we study the scaling relations or so-called Larson's laws for three MW-size galaxies with different morphologies. The article is organized as follows. Section 2 contains the description of our numerical model. Section 3 describes methods of cloud definition. In Section 4, we present a statistical analysis of the physical properties of molecular clouds. Section 5 describes the scaling relations and the dependence of the power-law indices of the relations on the threshold value and mass spectra of GMCs for the simulated galaxies. In Section 6, we summarize our key results.

2 MODEL

To simulate the galaxy evolution, we use our code based on the unsplit Total Variation Diminishing (TVD) Multi Upstream Scheme for Conservation Laws (MUSCL) scheme for gas dynamics and the *N*-body method for stellar component dynamics. In the gas dynamical approach, we reach second order in time and third order in space using the minmod limiter. For the Riemann problem solution, we adopt the Harten–Lax–van Leer–Contact (HLLC) method. More details about gas dynamic part of our code can be found in the article of Khoperskov et al. (2014). Stellar dynamics is calculated using the second-order flip-flop integrator. For the total stellar–gaseous gravitational field calculation, we use the TREECODE approach.

For all models presented here, we use a uniform grid with $4096 \times 4096 \times 512$ cells for gas dynamics and set a computational domain $40 \times 40 \times 3$ kpc with spatial resolution 6 pc. The initial number of stellar particles is equal to 0.5×10^6; during the simulation it reaches 2×10^6 depending on star formation activity.

2.1 Chemical kinetics and gas thermodynamics

Usually the emission in CO lines is a major source of information about GMCs (Dame, Hartmann & Thaddeus 2001; Bolatto et al. 2008; Leroy et al. 2009) and the intensity in CO lines is used to restore the mass of molecular hydrogen through the X_{CO} factor (Dickman 1975; Bolatto, Wolfire & Leroy 2013). We are thus interested in a reasonable CO chemical network that on one hand gives fine CO molecule evolution and on the other requires adequate computational resources. Rather detailed networks include more than 20 chemical species involved in several hundreds of reactions (e.g. Omukai 2000; Glover et al. 2010), which is computationally unacceptable for our purposes. Fortunately, Glover & Clark (2012) found that the reduced network proposed by Nelson & Langer (1999) gives adequate results in comparison with the detailed chemical model, which consists of 218 reactions amongst 32 species (Glover et al.

2010), so that here we exploit the model based on the network proposed by Nelson & Langer (1999).

Based on our simple model for H_2 chemical kinetics (Khoperskov et al. 2013), we expand the Nelson & Langer (1999) network by several reactions needed for hydrogen ionization and recombination. For H_2 and CO photodissociation, we use the approach described by Draine & Bertoldi (1996). The CO photodissociation cross-section is taken from Visser, van Dishoeck & Black (2009). In our radiation transfer calculation described in Section 2.3 below, we obtain the ionizing flux at the surface of a computational cell. To calculate self-shielding factors for CO and H_2 photodissociation rates and the dust absorption factor for a given cell, we use local number densities of gas and molecules, e.g. $f_{\rm sh}^{\rm H_2} = n_{\rm H_2} L$, where $n_{\rm H_2}$ is the H_2 number density in a given cell and L is its physical size. The chemical network equations is solved by the CVODE package (Hindmarsh et al. 2005).

We assume that a gas has solar metallicity, with the abundances given in Asplund, Grevesse & Sauval (2005): [C/H] $= 2.45 \times 10^{-4}$, [O/H] $= 4.57 \times 10^{-4}$ and [Si/H] $= 3.24 \times 10^{-5}$. Dust depletion factors are correspondingly equal to 0.72, 046 and 0.2 for C, O and Si. We suppose that silicon is singly ionized and oxygen stays neutral.

For cooling and heating processes, we extend our previous model (Khoperskov et al. 2013) using CO and OH cooling rates (Hollenbach & McKee 1979) and the C I fine structure cooling rate (Hollenbach & McKee 1989). The other cooling and heating rates are presented in detail in Appendix B in Khoperskov et al. 2013. Here we simply provide a list of the following: cooling due to recombination and collisional excitation and free–free emission of hydrogen (Cen 1992), molecular hydrogen cooling (Galli & Palla 1998), cooling in the fine structure and metastable transitions of carbon, oxygen and silicon (Hollenbach & McKee 1989), energy transfer in collisions with dust particles (Wolfire et al. 2003) and recombination cooling on dust (Bakes & Tielens 1994), photoelectric heating on dust particles (Bakes & Tielens 1994; Wolfire et al. 2003), heating due to H_2 formation on dust particles and H_2 photodissociation (Hollenbach & McKee 1979) and ionization heating by cosmic rays (Goldsmith & Langer 1978). In our simulations we achieve gas temperature values as low as 10 K and number densities as high as 5×10^3 cm^{-3}.

2.2 Star formation and feedback

In the star formation recipe adopted in our model, mass, energy and momentum from the gaseous cells where a star formation criterion is satisfied are transmitted directly to newborn stellar particles. A star particle is formed in a grid cell if the following criteria are fulfilled: (i) the gas density in the cell is higher than 100 cm^{-3} (such a high value prevents the formation of a huge number of stellar particles) and (ii) the total mass of gas in surrounding cells exceeds the Jeans mass $M_{\rm cell} > M_{\rm J}$ (this help us to avoid star formation in hot and warm media, where some feedback processes occur) and we adopt the local star formation efficiency 0.01. In star-forming cells, the number density and temperature reach $n >$ 200–500 cm^{-3} and $T \lesssim 50$ K.

The feedback model includes several sources of thermal energy, namely stellar radiation, stellar winds from massive stars and supernova (SN) explosions. The amount of injected energy connected to these processes is calculated for each stellar particle using the stellar evolution code STARBURST99 (Leitherer et al. 1999). We model supernova feedback only as thermal energy injection into a gas. We take into account mass loss by stellar particles due to SN explosions and stellar winds from both massive and low-mass stars.

2.3 Radiation transfer

To account for molecule photodestruction, we should know the spatial structure of the UV background in the galactic disc. Recent observations provide some evidence for significant radial and azimuthal variations of UV flux in nearby galaxies (Gil de Paz et al. 2007). No doubt such variations are stipulated by local star formation. We therefore need to include radiation feedback from stellar particles in our calculations.

Through our simulations, the UV emission of each stellar particle is computed with the stellar evolution code STARBURST99 (Leitherer et al. 1999), assuming solar metallicity of the stellar population, so that for each particle we know its luminosity evolution. After that, we separate particles into two groups: young stellar particles (the age is lower than 20 Myr) and others. For definiteness, we assume a uniform background field ten times lower than that in the Solar neighbourhood, $F_{\rm b} = 0.1$ Habing (erg cm^{-2} s^{-1}). Thus the UV background $F^{\rm UV}$ in a hydrodynamical cell with coordinates $\boldsymbol{r}_0$ can be written as

$$F^{\rm UV}(\boldsymbol{r}_0) = F_{\rm b} + \sum_i F_i^{\rm old}(r_0) + \sum_j F_j^{\rm young}(r_0, r_j)\,, \qquad (1)$$

where $\sum_i F_i^{\rm old}(r_0)$ is the deposit from the old stellar population (age >20 Myr), which plays a role only in a cell where a stellar particle is located ($\boldsymbol{r}_0$). The last term is the UV flux from the young stellar population: the brightest stars. Their deposit is the most important in the photodestruction of molecules in the surrounding medium.

Due to the number of young stars being small at each time step, we can use the ray-tracing approach for each stellar particle. For the jth 'young particle', we estimate the radius of a spherical shell (similar to the Strömgren sphere) where the UV field value decreases down to 0.1 Habing:

$$R_j^{\rm d} = 0.1\delta\sqrt{L_j^*/(4\pi)}\,, \qquad (2)$$

where L_j^* is the luminosity of the jth stellar particle in Habing units and $\delta = \sqrt{(\delta x)^2 + (\delta y)^2 + (\delta z)^2}$ is the effective cell size. For each shell, we calculate the UV flux assuming the optical depth $\tau = 2N/(10^{21}\,{\rm cm}^{-2})$, where N is the total column density of gas in cm^{-2}, so that we can obtain the distribution of UV intensity in the entire galactic disc according to equation (1).

2.4 Model of galaxies

We start our simulations from the self-consistent radial and vertical equilibrium state of stellar–gaseous discs in the fixed gravitational potential of a dark matter halo. We assume both stellar and gaseous discs have an exponential form, but with different spatial scalelengths. The circular velocity of the gaseous disc embedded in the gravitational potential can be found as

$$\frac{V_{\rm c}^2}{r} = -\left(\frac{\partial\Psi_{\rm halo}}{\partial r} + \frac{\partial\Psi_{\rm bulge}}{\partial r} + \frac{\partial\Psi_{\rm disc}}{\partial r} + \frac{\partial\Psi_{\rm gas}}{\partial r}\right)\,, \qquad (3)$$

where $\Psi_{\rm halo}$ is the gravitational potential of the dark matter halo, the halo is assumed to be a steady isothermal sphere, $\Psi_{\rm bulge}$ is the potential of the bulge, $\Psi_{\rm disc}$ is the potential of the stellar disc and $\Psi_{\rm gas}$ is the potential of the gas. The parameters of the gravitational potential can be found in Table 1. Fig. 1 presents the radial dependence of the circular velocity for the galactic models considered here.

Table 1. Initial parameters adopted in the simulations. Here, the following notations are assumed: $M_{\rm h}$ is the mass of dark matter halo within a 12-kpc sphere, $a_{\rm h}$ is the halo scale-length, $\sigma_r(0)$ is the central radial velocity dispersion, $\sigma_{\rm z}/\sigma_{\rm r}$ is the ratio of the vertical velocity dispersion to the radial one, $\Sigma_{\rm g0}$ is the central surface density of the gaseous disc, $h_{\rm g}$ is the radial scale-length of the gaseous disc, $N^{\rm th}_{\rm tot}$ is the number of clouds extracted with the $N^{\rm th}_{\rm CDN}$ threshold (CDN is a cloud definition when the total column density within the cloud exceeds the $N^{\rm th}_{\rm tot}$ threshold and the cloud is delineated by the corresponding level of total column density) and $N_{\rm CF}$ is the number of clouds extracted using CLUMPFIND (henceforth we use CF abbreviation for shortness). The following parameters are the same for the models considered: $\Sigma_{*0} = 835\,{\rm M}_\odot\,{\rm pc}^{-2}$ is the central stellar surface density, $h_* = 3$ kpc is the radial scale-length of the stellar disc and $h_\sigma{}^* = 2h_*$ is the radial velocity scale-length, where $\Sigma_{\rm g0} = 10\,{\rm M}_\odot\,{\rm pc}^{-2}$ is the central gas surface density.

Model (Morphology)	Halo		Bulge		Stellar disc		Cloud definition	
	$M_{\rm h}$ $10^{10}\,{\rm M}_\odot$	$a_{\rm h}$ kpc	$M_{\rm b}$ $10^{10}\,{\rm M}_\odot$	$b_{\rm h}$ kpc	$\sigma_{\rm r(0)}$ km s^{-1}	$\sigma_{\rm z}/\sigma_{\rm r}$	$N_{\rm CDN}$	$N_{\rm CF}$
B (No structure)	8.8	3.857	–	–	75	0.5	1095	1150
F (Milky Way-like)	8.8	1.1	0.7	0.153	100	0.7	1065	1203
H (Flocculent)	8.25	1.1	–	–	50	0.45	1012	1111

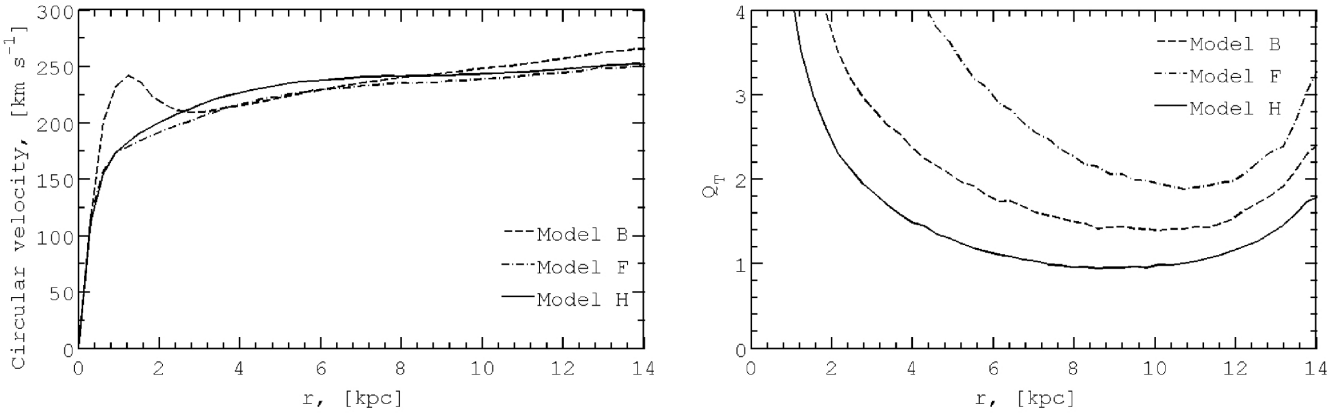

Figure 1. Initial conditions for simulated stellar–gaseous discs. Circular velocity is shown in the left panel. The stability parameter Q_T adopted for a finite-thickness two-component disc and using the approximation by Romeo & Wiegert (2011) is shown in the right panel. Physical parameters of galaxy models are presented in Table 1.

For stellar particle kinematics, the asymmetric drift is taken in the form of the Jeans approximation:

$$V^2 = V_{\rm c}^2 - \sigma_{\rm r}^2 \left(1 - \frac{\sigma_\varphi^2}{\sigma_{\rm r}^2} + \frac{r}{\Sigma_*}\frac{1}{\sigma_r^2}\frac{\partial(\Sigma_*\sigma_{\rm r}^2)}{\partial r}\right), \quad (4)$$

where $\sigma_{\rm r}$ and σ_φ are radial and azimuthal velocity dispersions, respectively, and Σ_* is the stellar surface density distribution. The parameters of the potential and matter distributions can be found in Table 1. To compute an initial distribution of stars, we solve equation (4) using the iterative procedure described in Khoperskov, Zasov & Tyurina (2003).

Despite the parameters of the galaxy models presented in Table 1 being close to each other, the various stability conditions allow us to follow galaxies with different morphologies. Initial stability criteria for two-component models (stellar–gaseous) are shown in the right panel of Fig. 1. We compute three models of the stellar disc equilibria: a gravitationally overstable disc (Model F, without prominent structure), highly unstable (Model H, flocculent spiral morphology) and an intermediate-state disc (Model B, MW-like morphology). The initial stability parameter for the two-component disc model accounting for the finite disc thickness effect is adopted in the form used by Romeo & Wiegert (2011) (Fig. 1).

Fig. 2 shows maps of the stellar surface density, stellar UV radiation field, total gas column density and CO integrated intensity at $t = 500$ Myr for the following models of galaxies inclined by $i = 30^\circ$: a galaxy without spiral structure (model B), a MW-type galaxy (model F) and a flocculent galaxy (model H). The initial parameters of the models are given in Table 1. Note that the spatially averaged UV radiation field in all three models of galaxies is significantly greater than a value of 0.1 Habing (see upper middle row in Fig. 2), so that our choice of a uniform background is reasonable. We have adopted inclination angle $i = 30^\circ$ as a value that is enough to obtain significant line-of-sight velocity scatter while the structures in the gaseous disc are still fairly spatially distinguishable.

3 CLOUD DEFINITION

Prior to the calculation of the physical parameters of clouds, we should define what a cloud is. In the most obvious approach for cloud definition (CD), a cloud is an isolated gaseous clump with gas density (column or volume) higher than a given level. This is the simplest criterion, but it does not reflect the chemical composition of a clump and we cannot say anything about the molecular content of such a cloud. Moreover, methods based on the total gaseous column density are not relevant to observable values, because, when using such methods, some material that is not associated with the cloud itself and is laid along the line of sight can be regarded as part of a cloud. This is revealed in the physical parameters of a cloud. We therefore need a criterion based on the distribution of molecules in the ISM. Such a criterion connects both chemical and extinction

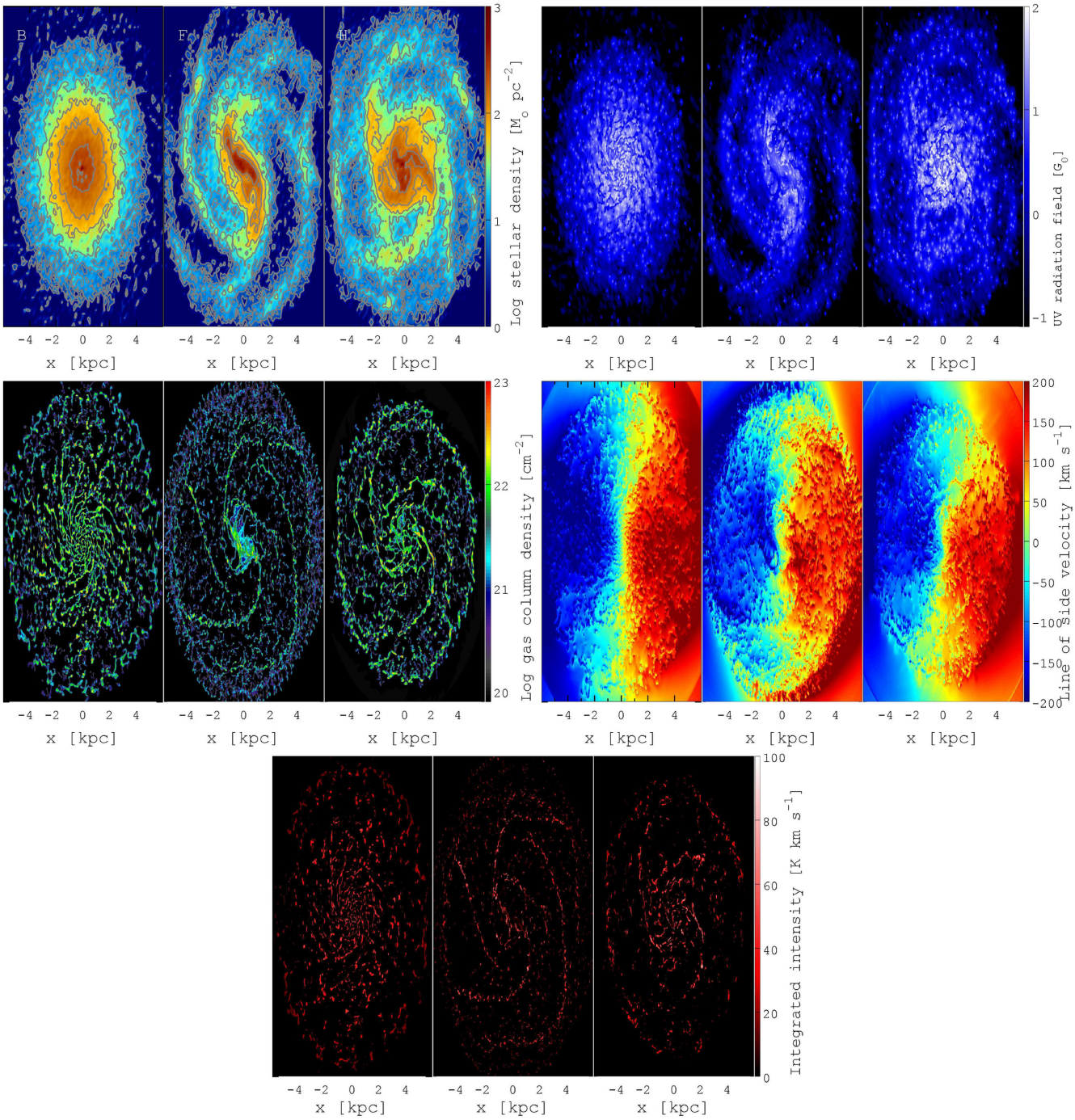

Figure 2. Projected maps (inclination 30°) of stellar surface density (top left group of panels), stellar UV radiation field (top right group of panels), total gas column density (left group of panels in the middle row), radial (line-of-sight) velocity component (right group of panels in the middle row) and CO integrated intensity (bottom group of panels) at $t = 500$ Myr for the following models of galaxies: no spiral structure or model B (left map in all groups of panels), MW-like or model F (central map in all groups of panels) and flocculent galaxy or model H (right map in all groups of panels). Initial parameters of the galactic models can be found in Table 1.

properties of a cloud and allows us to separate the two phases of the cold interstellar medium: atomic and molecular gas.

Usually, molecular clouds are studied through their emission in molecular lines (e.g. ^{12}CO (see e.g. Solomon et al. 1987), ^{13}CO (see e.g. Heyer et al. 2009) and more recently OH (Allen, Hogg & Engelke 2015)). Since our model includes the H_2 and CO molecule kinetics, we can use CD criteria based on both total gas column density and intensity in CO lines. This allows us to check the range of applicability for each CD criterion. The properties of a particular cloud are therefore expected to depend significantly on the extraction criterion. It is also unclear how the choice of criterion influences the statistical properties of the whole ensemble of molecular clouds.

Below, we consider two approaches related to the properties of a cloud measured in observations. We define a cloud as a region inside which the total (molecular and atomic) hydrogen column density is higher than a given threshold $N_{\rm tot}^{\rm th}$ (henceforth we use

the abbreviation CDN for the method and corresponding indices). According to the CDN criterion, we first find all local maxima (peaks) of the gas column density in the plane of the galactic disc. After that, around each local maximum we find cells with value higher than a given threshold. In some cases, these regions merge into larger ones and form a cloud with several local maxima. Usually such coalescences take place in dense galactic structures, e.g. in spiral arms, a bar or regions near the galactic centre. Thus, our approach for finding clouds is a combination of the '*contour method*' (Fujimoto et al. 2014) and '*peaks method*' (Tasker & Tan 2009).

One of the widely used methods for extracting structures from PPV data cubes is CLUMPFIND (Williams et al. 1994). This method is based on contouring a data array at many different levels starting from the peak value and moving down to a specific threshold. In the present work, the CUPID implementation of the CLUMPFIND algorithm is used for the CO intensity method of cloud extraction (Berry et al. 2007). Henceforth we use the abbreviation CF for this method and the corresponding indices of variables.

We calculate the CO brightness temperature in the form of PPV data cubes using the method described in Feldmann, Gnedin & Kravtsov (2012). In the calculations, the spectral velocity resolution equals 0.5 km s^{-1}, which is potentially enough to resolve the structure of massive clouds. This spectral resolution is comparable to the one reached in recent interferometric observations (see e.g. Roman-Duval et al. 2009). Note that we discuss the dependence of the power-law indices of the relations on the velocity resolution value in Section 5.4.

Certainly, using the two above-mentioned criteria, we obtain two different populations of clouds. The number and total mass of clouds are also different and depend on the value of column density and the brightness temperature thresholds. In our analysis, we take $N_{\rm tot}^{\rm th} = 1.9 \times 10^{21}$ $\rm cm^{-2}$ and $T_{\rm b}^{\rm th} = 3$ K as fiducial threshold values, which provides us with comparable numbers of clouds (around 1000) and similar total gaseous masses locked in clouds ($M_{\rm t} \approx 2$–4×10^9 $\rm M_\odot$). Note that these values of $M_{\rm t}$ are close to the total mass of molecular clouds in the MW (Williams & McKee 1997). The numbers of clouds and total gaseous masses for the galactic models considered here are given in Table 1.

For instance, a small region with the spatial distribution of extracted clouds in the MW-type galaxy (model F) is shown in Fig. 3. We mark the extracted clouds as coloured areas, in contrast to the grey-scale background of the gaseous column density map. It is clearly seen that spatial distributions and numbers of clouds are remarkably distinct for the criteria considered. Prior to any quantitative analysis of the physical parameters, we should notice two issues. On one hand, non-interacting clouds appear to have a similar shape for both extraction methods. However, in a more dense environment clouds extracted by different methods look very unlikely. We suppose that this can be a result of dynamical effects related to cloud collisions and/or stellar feedback effects. On the other hand, it seems that very large clouds (or agglomerations) extracted using the CDN method have internal structure, which we can barely resolve because our spatial resolution is still not high enough. Thus, for the CDN criterion, large clouds and cloud chains (at least in the dense environment) can be extracted, while using the CF method such large structures are split into individual lumps with internal motions and other specific inhomogeneities.

4 GMC PHYSICAL PARAMETERS

Cloud formation was studied numerically in detail by Dobbs, Bonnell & Pringle (2006), Dobbs et al. (2008) and Dobbs (2008).

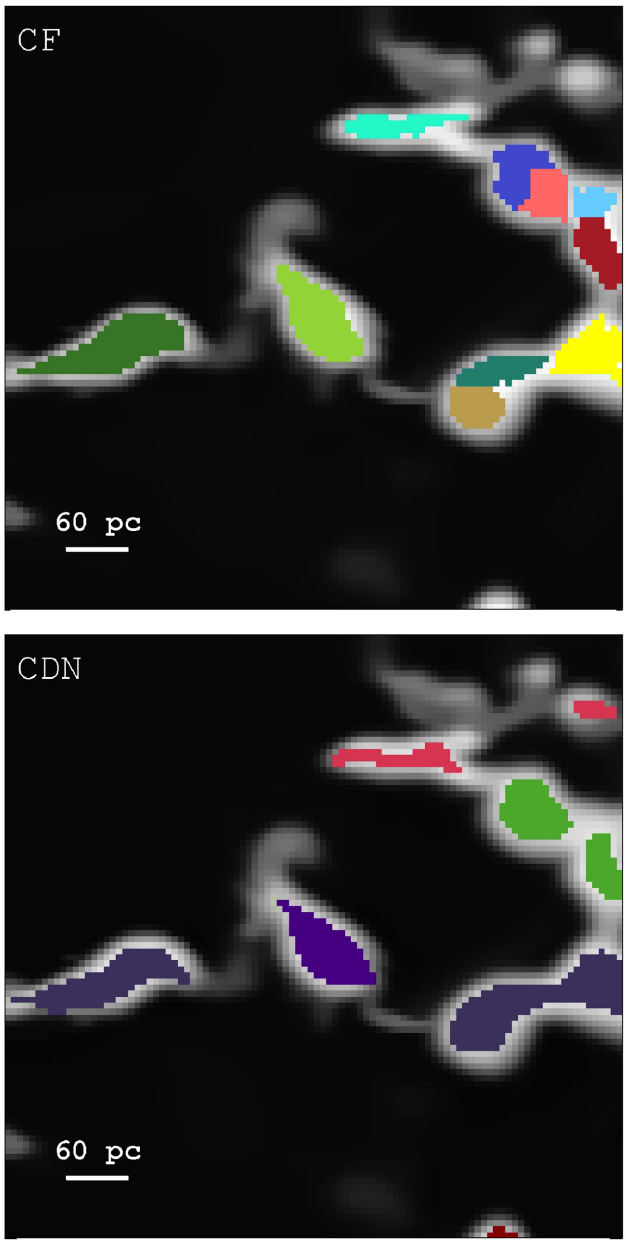

Figure 3. A region with the spatial distribution of extracted clouds in model F. The extracted clouds are marked by colour: the top panel shows the distribution for the CF (or CLUMPFIND) method, while the bottom panel demonstrates that for the CDN approach. The background grey-scale map is the gas surface density.

We mention that in our simulations clouds are the result of self-gravity, thermal instability, cloud collisions and other processes occuring in the galactic disc. Here we briefly describe the physical parameters of the cloud samples obtained in our analysis.

On one hand, spiral arms stimulate GMC formation due to gas falling into the gravitational potential well of the arms. The gravitational potential of the spiral structure induces collisions of clouds, which in turn stimulates star formation. On the other hand, supernova explosions in star-forming spiral arms can destroy clouds. One can therefore conclude that molecular clouds mostly form in spiral arms and are probably short-lived structures with lifetimes $\lesssim 10^7$ yr (Roman-Duval et al. 2009; Meidt et al. 2015). However, the existence of clouds in the inter-arm regions requires a longer lifetime

(Scoville, Solomon & Sanders 1979; Koda et al. 2009), so that the question of the lifetime of molecular clouds is still under debate (see e.g. Dobbs & Pringle 2013; Zasov & Kasparova 2014).

The number of clouds extracted by using both criteria for the cloud definition described above depends on the choice of threshold. For the fiducial values of threshold $N_{\rm tot}^{\rm th} = 1.9 \times 10^{21}$ cm^{-2} and $T_{\rm b}^{\rm th} = 3$ K, we extract ∼1000 isolated clouds in our simulated galaxies. These clouds have the following physical parameters: masses are ≈10^4–10^7 M$_\odot$, sizes vary within the range 3–100 pc, one-dimensional velocity dispersion is in the range 0.1–10 km s^{-1}, mean surface densities are ∼60–300 M$_\odot$ pc^{-2} and luminosities in CO lines are 10^3–10^7 K km s^{-1} pc^2. These parameters depend slightly on the galactic morphology. Fig. 4 shows the distributions of these physical parameters for the cloud population in the MW-type galaxy (Model F) for both techniques of cloud definition.

For the CF method, the physical parameters of clouds, i.e. masses, 1D line-of-sight velocity dispersion (LOSVD), total luminosity and cloud sizes, are calculated using the prescriptions from Williams et al. (1994).

For the CDN approach, the one-dimensional velocity dispersion of a cloud is calculated according to

$$\sigma_v = \frac{1}{\sqrt{3}} \sqrt{\sum (\boldsymbol{u} - \boldsymbol{u}_{\rm c})^2}\,, \tag{5}$$

where $\boldsymbol{u}_{\rm c}$ is the cloud centre mass velocity vector and $\boldsymbol{u}$ is the cloud velocity vector. Such an approach is widely used to extract clouds in numerical simulations (see e.g. Benincasa et al. 2013; Fujimoto et al. 2014, and references therein). The cloud size is calculated according to $R = \sqrt{\frac{A}{\pi}}$, where A is the cloud surface in pc^2.

The ratio between the kinetic energy and gravitational energy is commonly used to specify the deviation from the virial state of a cloud under the assumption of a constant density distribution (Bertoldi & McKee 1992):

$$\alpha = \frac{5\sigma_{\rm v}^2 R_{\rm cl}}{G M_{\rm lum}} \approx \frac{1161\sigma_{\rm v}^2 R_{\rm cl}}{M_{\rm lum}}\,, \tag{6}$$

where α is the cloud virial parameter, $R_{\rm cl}$ is the cloud size in pc and $M_{\rm lum}$ is the mass of the cloud in solar units adopted from its CO luminosity using the $X_{\rm CO}$ conversion factor (Dickman 1978):

$$M_{\rm lum} = \frac{4.4 L_{\rm CO} X_{\rm CO}}{2 \times 10^{20}}\,. \tag{7}$$

It is easy to see that the luminosity mass $M_{\rm lum}$ and virial mass $M_{\rm vir}$ of a cloud are generally not equal to each other:

$$M_{\rm vir} \approx \alpha M_{\rm lum}\,. \tag{8}$$

The middle panels in Fig. 4 present the parameter α for the cloud population in the MW-type galaxy. It is clearly seen that the majority of molecular clouds tend to be in virial equilibrium. Note that the distribution of such quasi-virialized objects is close to a uniform distribution as a function of cloud mass. The physical parameters obtained for our models of galaxies are in agreement with other recent numerical simulations (Tasker & Tan 2009; Tasker 2011; Khoperskov et al. 2013). Such a result is likely to be a reflection of the turbulent energy distribution in the entire galactic disc (see the detailed study in Kraljic et al. 2014).

The distributions of cloud masses obtained using the CF and CDN methods are slightly different: in the former, we extract smaller and less massive clouds than the ones extracted in the latter (see Fig. 4a and b). Moreover, the mass range for the CF sample of clouds is rather wide. The reason for this is clearly seen in Fig. 3: large structures extracted by the CDN method are divided into several smaller clouds when the CF technique is used (see Fig. 3). We discuss several dynamical and methodological effects related to this issue in the following paragraphs.

The 1D velocity dispersion of clouds defined by equation (5) is unlikely to provide a good description for the observed line-of-sight velocity dispersion, making it higher, at least for extragalactic GMCs. Moreover, the regular quasi-circular motion of giant clouds around the galactic centre leads to overestimation of velocity field within a cloud by about 1–2 km s^{-1}. However, this effect is significantly smaller than the 1D LOSVD value. A spectral resolution of 0.5 km s^{-1} allows us to distinguish the internal structure of large clouds and measure the 1D LOSVD within a 1–2 km s^{-1} accuracy (see Fig. 4e). Using the CF method, we extract a more homogeneous cloud sample, which has a smoother (without many local peaks) distribution. In any case, both methods provide a more-or-less similar shape for the velocity dispersion distribution functions, which are close to the observable ones (see e.g. Roman-Duval et al. 2010). It seems that the CF method splits large clouds into smaller ones due to the complex velocity structure, which mainly occurs in colliding and tangent gaseous flows or, in general, in turbulent regions. Note a remarkable difference between clouds extracted by the CF and CDN methods: large clouds found by the CF method are isolated lumps located in a calm environment, whereas large clouds extracted using the CDN criterion mostly represent dynamically interacting structures.

5 SCALING RELATIONS ANALYSIS

In this section, we discuss the scaling relations for GMCs extracted according to two criteria of cloud definition for the galaxy models described above. In Table 2, we collect all indices and normalizations for the scaling relations obtained in the analysis of the galaxy models considered here. It seems that there is no strong variation of the GMC scaling relations obtained using the CDN method for galaxies with different morphology. This is considered in detail in Sections 5.1, 5.2 and 5.3. The role of the environment in the galactic disc as regards the GMC parameters is discussed in Section 5.6.

The statistical relations for the three models of galaxies considered here are presented in Figs 5, 6 and 7 and described in the corresponding subsections. The top row of panels in each figure shows the relations obtained using the CF method and the bottom one shows the relations based on the CDN criterion.

5.1 Velocity dispersion–size relation

Fig. 5 shows that the clouds extracted according to the CDN criterion have higher velocity dispersion, with mean value ∼8–20 km s^{-1}, compared with that obtained for the CF criterion; in this case, the mean value of velocity dispersion decreases to ∼1–5 km s^{-1}. One can note that the observational fits for the MW galaxy and others (Solomon et al. 1987; Bolatto et al. 2008) are in better agreement with the relations obtained for the CF sample of clouds. The relations for the clouds extracted by the CDN method show significant deviation from the observational fits.

Clouds have extremely complicated shapes and consist of crossed and elongated structures (see Fig. 3), so that high total hydrogen column density at the periphery of clouds can be a geometrical effect when the line of sight lies along the largest dimension of the cloud. Use of the CDN criterion can therefore result in incorrect estimation of cloud sizes and overestimation of their column density and velocity dispersion (Fig. 4).

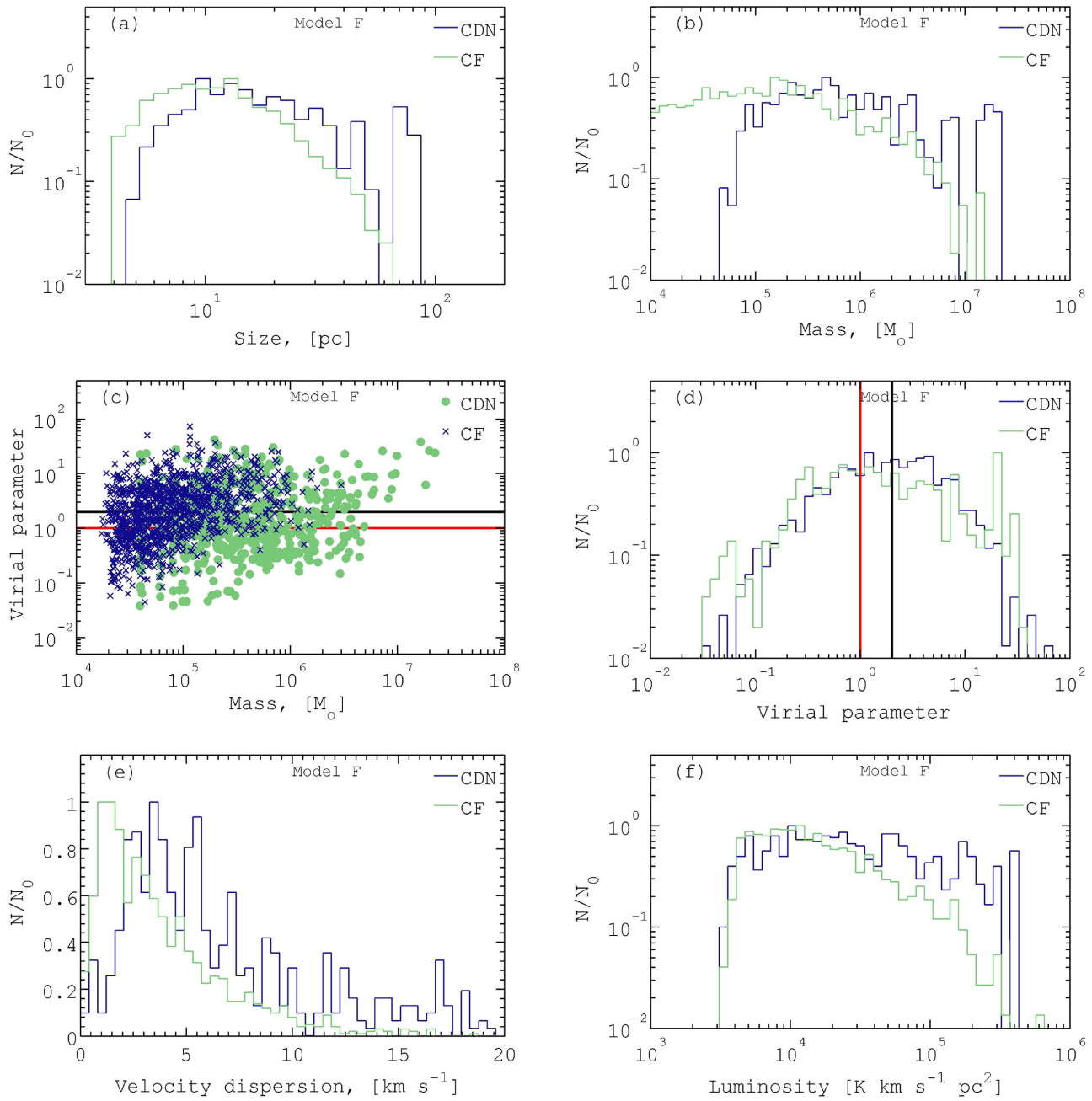

Figure 4. The physical parameters of GMCs obtained using the CDN criterion (bright blue) and CLUMPFIND algorithm (light green) for the model F galaxy (middle panel of Fig. 2): (a) size, (b) mass, (d) virial parameter, (e) velocity dispersion and (f) luminosity. The dependence of the virial parameter on the mass of a cloud is shown in panel (c). The red dotted and black solid lines depicted in panels (c) and (d) correspond to $\alpha = 1$ and $\alpha = 2$, respectively.

From the bottom panels in Fig. 5, one can conclude that, for the column density threshold adopted here, the clouds extracted using the CDN criterion hold gas with higher velocity located at their periphery. Such intercloud (diffuse) gas can contain a significant molecular fraction. Note that in some recent observations extended structures with significant molecular fraction are found around molecular clouds (Caldú-Primo et al. 2015). The velocity dispersion of these structures is higher than that in the clouds. This can be considered as evidence that molecular gas can exist in two phases: the clumpy phase, which is organized in molecular clouds, and the diffuse one, which is located in extended structures around clouds.

CO molecules are formed efficiently only in the dense shielded environment and are destroyed due to heating and photodissociation by stellar feedback. Using the CDN criterion, total hydrogen column density has a deposit not only from central dense molecular regions, but also from the peripheral parts of a cloud, which mainly contain atomic hydrogen and even some intercloud star-forming regions, where young stars already exist. If we extract clumps emitting brightly in CO lines, then the low-density H I gas at the periphery is excluded from consideration.

One can see that the indices in the power-law relation σ_v–R_{cl} for models of galaxies with more pronounced structures differ significantly from those for the observational fits (Larson 1981; Solomon

Table 2. Parameters of the scaling relations for GMCs in simulated galaxies.

Model (Morphology) – CD	$\sigma_v = A_1 R_{cl}^{\beta_1}$		$M_{vir} = A_2 L_{cl}^{\beta_2}$		$L_{cl} = A_3 R_{cl}^{\beta_3}$	
	A_1 km s^{-1} pc$^{-\beta_1}$	β_1	A_2 M$_\odot$ (K km s^{-1} pc^2)$^{-\beta_2}$	β_2	A_3 K km s^{-1} pc^2 pc$^{-\beta_3}$	β_3
B (No structure) – CDN	0.94 ± 0.25	0.66 ± 0.17	795 ± 151	0.64 ± 0.31	200 ± 45	1.72 ± 0.13
B (No structure) – CF	0.97 ± 0.12	0.49 ± 0.1	15.8 ± 2.2	1.56 ± 0.11	1000 ± 38	1.02 ± 0.2
F (Milky Way-like) – CDN	0.35 ± 0.21	1.11 ± 0.18	16 ± 8.1	1.04 ± 0.28	202 ± 29	1.73 ± 0.11
F (Milky Way-like) – CF	0.57 ± 0.18	0.69 ± 0.12	13.1 ± 3.6	1.47 ± 0.21	630 ± 44	1.28 ± 0.19
H (Flocculent) – CDN	0.87 ± 0.24	0.76 ± 0.16	1584 ± 212	0.62 ± 0.29	156 ± 51	1.68 ± 0.3
H (Flocculent) – CF	0.84 ± 0.9	0.54 ± 0.09	16.2 ± 3.1	1.56 ± 0.1	1000 ± 35	1 ± 0.21

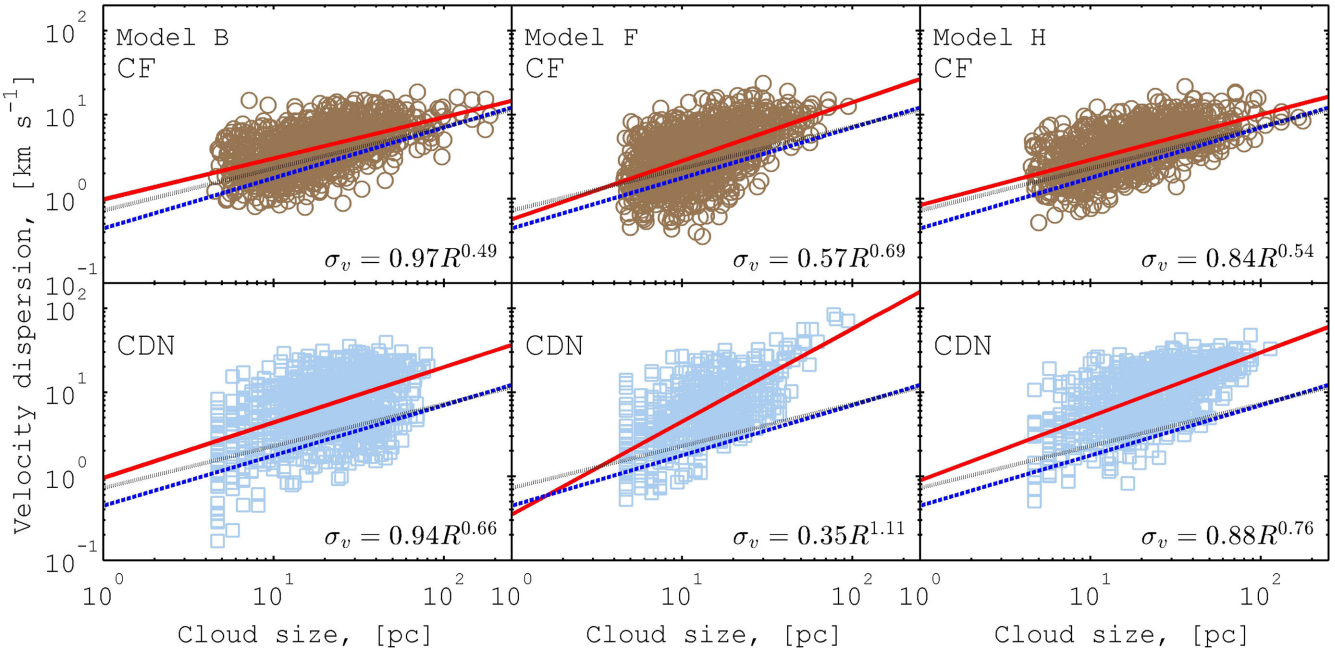

Figure 5. The 'velocity dispersion–cloud size' relation obtained for the CF algorithm (top row of panels) and the CDN criterion (bottom row of panels). The left column of panels corresponds to the model of a galaxy without spiral structure (model B), the middle column presents the relation for the MW-like galaxy model (model F) and the right column shows the relation for a galaxy with flocculent structure (model H, see Fig. 2). The solid red line is a power-law fit for the simulated data (the corresponding formula is shown in the right bottom corner). The dashed blue line corresponds to the fit for the data taken from Bolatto et al. (2008). The dotted black line shows the fit to the data on the MW clouds obtained by Solomon et al. (1987).

et al. 1987; Bolatto et al. 2008). This deviation takes place for both threshold criteria, but is smaller for the CF method. This can be explained by the fact that, using the CDN criterion, we can consider gaseous structures that are not really associated with clouds, so that gaseous flows at the outskirts of a cloud are added to the internal turbulence motions of this cloud and hence the numerical ratio between velocity dispersion and cloud size becomes higher. We mentioned above that the CF approach is a sharper 'filter' for molecular clouds than the CDN one and our cloud samples based on CO data cubes data demonstrate statistical relations closer to the observed ones. Thus, in our simulations the first Larson's scaling relation is reproduced better for PPV data.

5.2 Virial mass–luminosity relation

The 'virial mass–luminosity relation' reflects a suggestion that the GMC state is close to virial equilibrium. Fig. 6 shows the correlation between virial mass M_{vir} (see equation 8) and total luminosity of the extracted molecular clouds for three models of galaxies. One can see significant scatter of the physical parameters for the simulated clouds around the observational fits. Similarly to the 'velocity dispersion–size' relation, one can see here also that the scatter for the CDN criterion is larger than that for the CF one; this is especially remarkable for low surface luminosity clouds ($L_{CO} \lesssim 10^4$ K km s^{-1} pc^2). In general, for the same luminosity value, the virial mass of clouds obtained for the CDN criterion is systematically greater than that for the CF one. That can be explained by the fact that high virial masses have large clouds formed in collisions of smaller ones; such massive clouds are mainly associated with spiral arms and/or bar. During collisions of clouds, molecules can be destroyed but the shock waves cannot ionize gas (or such gas recombines rapidly), so that a significant part (by mass) of such clouds is locked in the warm atomic hydrogen phase. Then, using the CDN criterion we obtain clouds with high total hydrogen column density, where the deposit of atomic hydrogen to the column density is dominant or very significant.

The CO brightest clouds are really molecular ones and they probably belong to an older cloud population – the gas inside them has to become molecular (Glover et al. 2010) – whereas the darkest (massive) clouds in the CO line are believed to be either a young population of massive clouds, in which atomic hydrogen has not yet transformed into molecular, or perhaps pseudo-virialized structures,

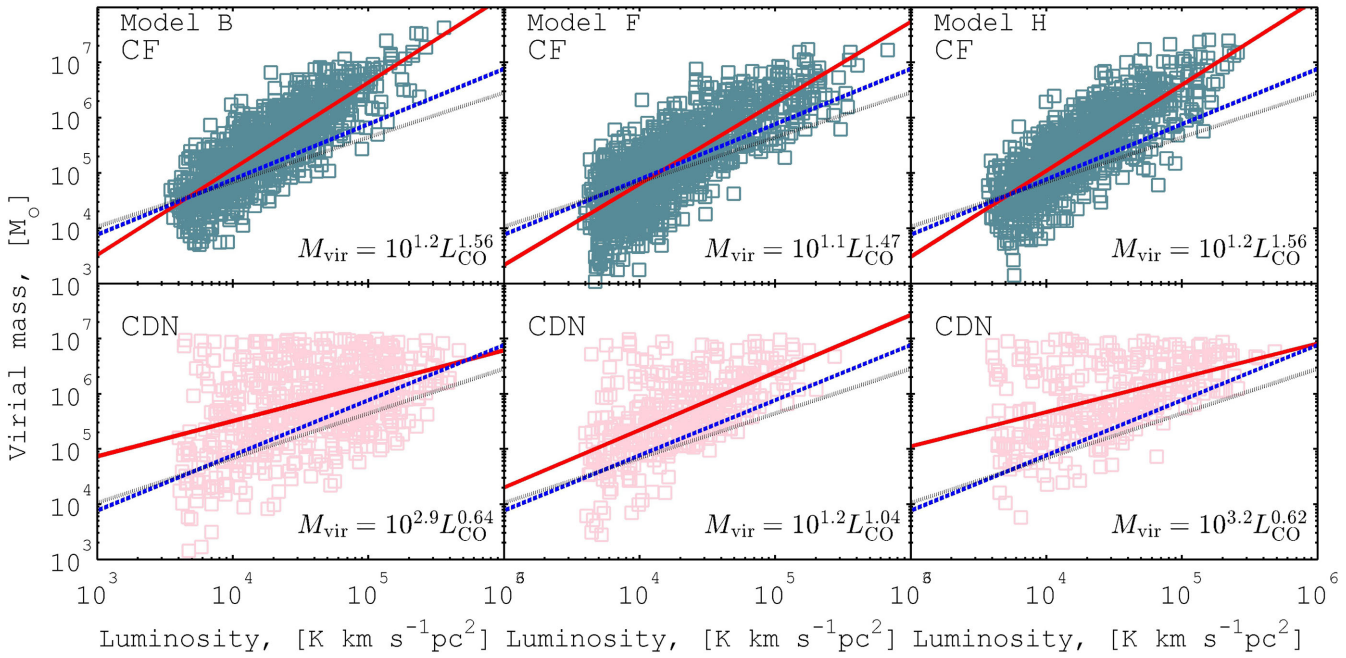

Figure 6. The 'cloud virial mass–luminosity' relation. The other notations are the same as in Fig. 5.

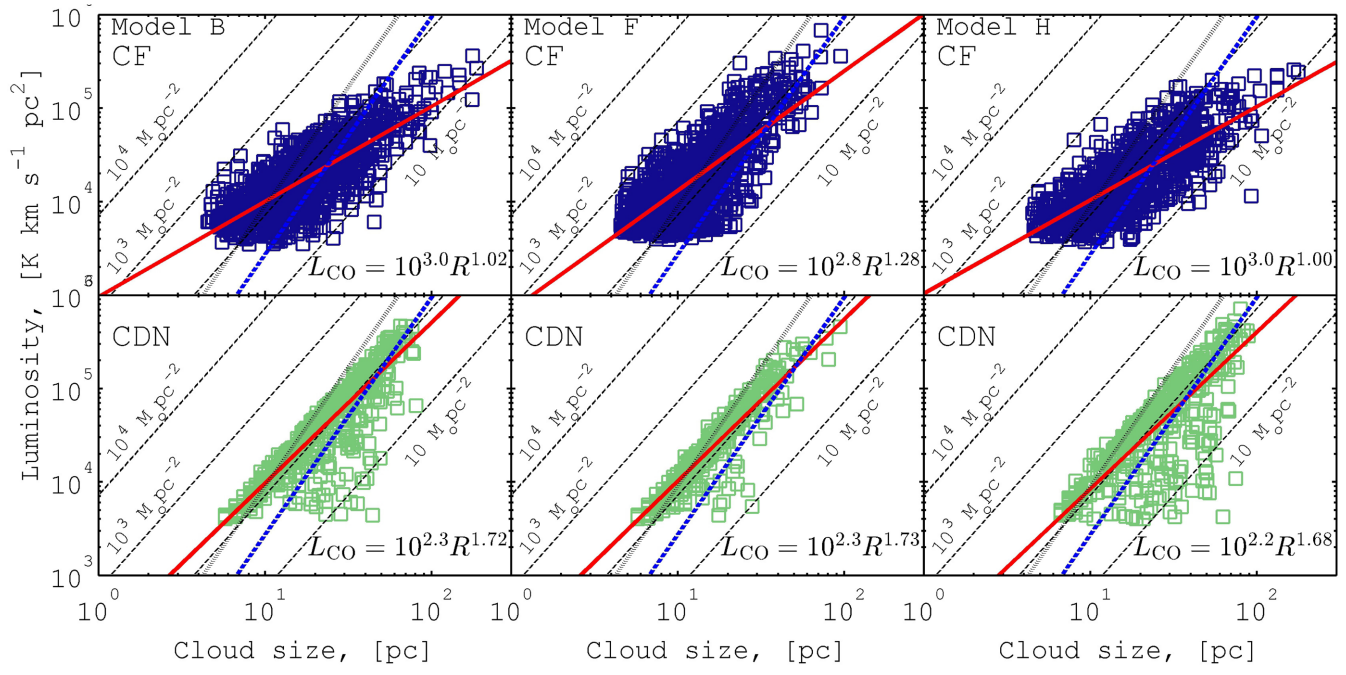

Figure 7. The 'luminosity–cloud size' relation. The dotted lines correspond to the cloud surface density according to equation (7) for the constant conversion factor $X_{\rm CO} = 2 \times 10^{20}$ cm^{-2} (K km s^{-1})$^{-1}$. The other notations are the same as in Fig. 5.

which consist of a group of small molecular clouds 'bounded' by an atomic intercloud and/or more diffuse molecular medium (see Fig. 3). Such structures can appear in dense environment, e.g. spiral arms, bar or the central parts of a galaxy, where the chosen threshold is low enough to extract separate clouds and leads to mergers of small clouds into larger structures. The use of the CF criterion provides a more reasonable cloud sample and does not lead to extraction of such large gaseous structures, so that the scatter for the sample of clouds obtained for the CF criterion is much smaller than for the CDN one.

For the CDN criterion, the slope of the fit for the simulated sample of clouds is flatter than that for the observational data (see Fig. 6). Obviously, it comes from the excess of massive clouds with low surface luminosity. Using the CF approach, the picture for all three models of galaxies shows opposite behaviour. The slope becomes steeper than that obtained in the observations. Above, one can see that the CF method usually leads to splitting large structures into smaller ones due to systematic line-of-sight velocity variations for a given structure (see Fig. 3), something revealed in both size and mass distributions (see Fig. 4). Thus, we have a relatively large

subsample of small clouds, which cannot be resolved (in space and/or in the line-of-sight velocity coordinate) in observational data.

One can suppose that if a large gaseous agglomeration in the vicinity of spiral arms or the galactic centre is split into several isolated clouds, then the number of massive and bright clouds becomes lower, whereas smaller clouds are more numerous. Thus, the slope of the fit can become flatter, so that the increase of threshold value is likely to result in a better match with observations.

5.3 Luminosity–size relation

Originally, Larson (1981) found the 'mass–size' relation for Galactic molecular clouds: $M_{\rm cl} \propto R_{\rm cl}^2$. This relation can be interpreted as molecular clouds having the same (constant) surface density. Here we use another form of this relation, namely 'luminosity–size', because it includes at least one observable value. Note that the mass of a cloud can be easily found from the luminosity using the conversion factor $X_{\rm CO}$ according to equation (7); such recalculation does not affect the slope of the scaling relation in the case of a constant conversion factor.

Fig. 7 shows the relation for three models of galaxies. It is clearly seen that for all models the surface density of clouds is locked within interval ∼10–1000 $\mathrm{M_\odot\ pc^{-2}}$. This surface density range is universal within $M = 10^3$–10^7 $\mathrm{M_\odot}$ for all galaxy models. For the CDN criterion, one can note the substantial scatter of cloud parameters below a critical value of surface density $\approx 10^2$ $\mathrm{M_\odot\ pc^{-2}}$ (see the bottom row in Fig. 7). This is just a reflection of the existence of dimmer parts of the clouds. It seems that the strong limit on the maximum value of surface density can be interpreted as a result of ongoing star formation, which prevents the formation of more dense clouds. Molecules in such clouds are destroyed immediately, due to photodissociation by UV radiation from newborn stars. However, such a picture cannot be supported by the analysis of the clouds extracted by the CF method (see top row in Fig. 7). It is possible that the brightness of large clouds becomes lower than that expected due to shielding effects. Note that optical depth effects become important when the value of the column density exceeds $\sim 2 \times 10^{21} (T/10^3)^{-1}$ $\mathrm{cm^{-2}}$ (e.g. Hollenbach & McKee 1979) and the dense parts of clouds become dimmer in the CO lines.

Note that in our simulations the gas number density can be high as 2000–3000 $\mathrm{cm^{-3}}$. However, even in such a dense medium a star does not necessarily form, because the gas can be in equilibrium with the surrounding medium. Such a picture is usually found in small clouds, so that sometimes one can find rather small clouds (see Fig. 4a and b) with a large amount of molecular gas and these clouds appear to be brighter than expected from the third Larson's relation. Thus, in our calculations the cloud surface density is expected not always to be constant, which reflects the fact that in our model there is no gas density threshold for the star formation process.

5.4 Variation of spectral resolution

The spatial resolution in numerical simulations plays a significant role in our understanding of the internal properties and basic physical parameters of GMCs. Fujimoto et al. (2014) reported that the variation of spatial resolution strongly affects the properties of cloud populations. At the same time, the results of PPV data cube analysis can depend on spectral resolution. In our previous simulations of synthetic spectra, the velocity resolution equals $\delta v = 0.5$ $\mathrm{km\ s^{-1}}$, which is quite high for extragalactic observations. Although this value is comparable to that used in several studies (e.g. Tan et al. 2013), most of the recent extragalactic surveys in molecular lines have been performed with much lower spectral resolution (Engargiola et al. 2003; Donovan Meyer et al. 2013; Schinnerer et al. 2013; Combes et al. 2014).

Table 3. Power-law indices of the scaling relations found in Model F for several values of CO spectral line resolution δv.

Model/Observations	δv km s^{-1}	β_1	β_2	β_3
Larson (1981)	–	0.38	–	–
Bolatto et al. (2008)		0.5	0.81	2.55
Solomon et al. (1987)		0.6	1	2.54
Roman-Duval et al. (2010)	1	–	–	2.36
Model F	0.5	0.69	1.47	1.28
Model F	1	0.65	1.34	1.74
Model F	5	0.6	1.19	2.41

To check whether spectral resolution affects the scaling relations, we calculate and analyse PPV data with lower spectral resolution, $\delta v = 1$ and 5 $\mathrm{km\ s^{-1}}$, for model F. In Table 3, we show the power-law indices for scaling relations with different resolution values; we also combine the indices obtained in several observations with brightness temperature threshold equal to 1 K. We argue that the noticeable variations of the indices with δv are due to the fact that for lower spectral resolution small clouds are combined into larger ones along the line of sight when their relative motion and velocity dispersion are lower than or comparable with the spectral resolution. Here, we only report that there is a dependence of the cloud population characteristics on spectral resolution. An accurate quantitative consideration of this effect requires further detailed study.

5.5 Variation of the threshold value

In the previous subsections, we have established that the scaling relations for the cloud ensembles obtained in our simulations are quite similar to those found in observations. It is interesting to study the dependence of the power-law indices of the relations on the threshold value.

We consider the relations obtained by both methods described in Section 3. Here we constrain ourselves to analysing the model of a galaxy with prominent structure – model F. To do this, we vary threshold values in the following ranges: $N_{\rm tot}^{\rm th} = (0.5 - 4) \times 10^{22}$ $\mathrm{cm^{-2}}$ for CDN and $T_{\rm b}^{\rm th} = (1 - 15)$ K for CF. Using the lower limits, we extract clouds with mass less than 10^8 $\mathrm{M_\odot}$, while for the upper values at least 100 molecular clouds remain in the catalogue.

Fig. 8 presents the dependence of the power-law indices for the three scaling relations on total column density threshold $N_{\rm tot}^{\rm th}$ (left panels) and brightness temperature $T_{\rm b}^{\rm th}$ threshold (right panels). The error bars correspond to the data dispersion obtained in the χ^2-fitting procedure of the power-law indices for a given threshold. Note that the number of clouds definitely depends on the threshold value, but it remains above 100 clouds in order to provide enough objects for statistics.

For low $N_{\rm tot}^{\rm th}$, we extract both extremely large and small clouds. Large clouds consist of a group of small clouds enclosed by extended diffuse structure, which can be called the intercloud medium. Such a structure includes both molecular and atomic gas. Increasing the threshold excludes the intercloud medium, so that for higher threshold values we extract the bright cores of virialized clouds. One can see in Fig. 8 (left panels) that the indices β_i for the simulated

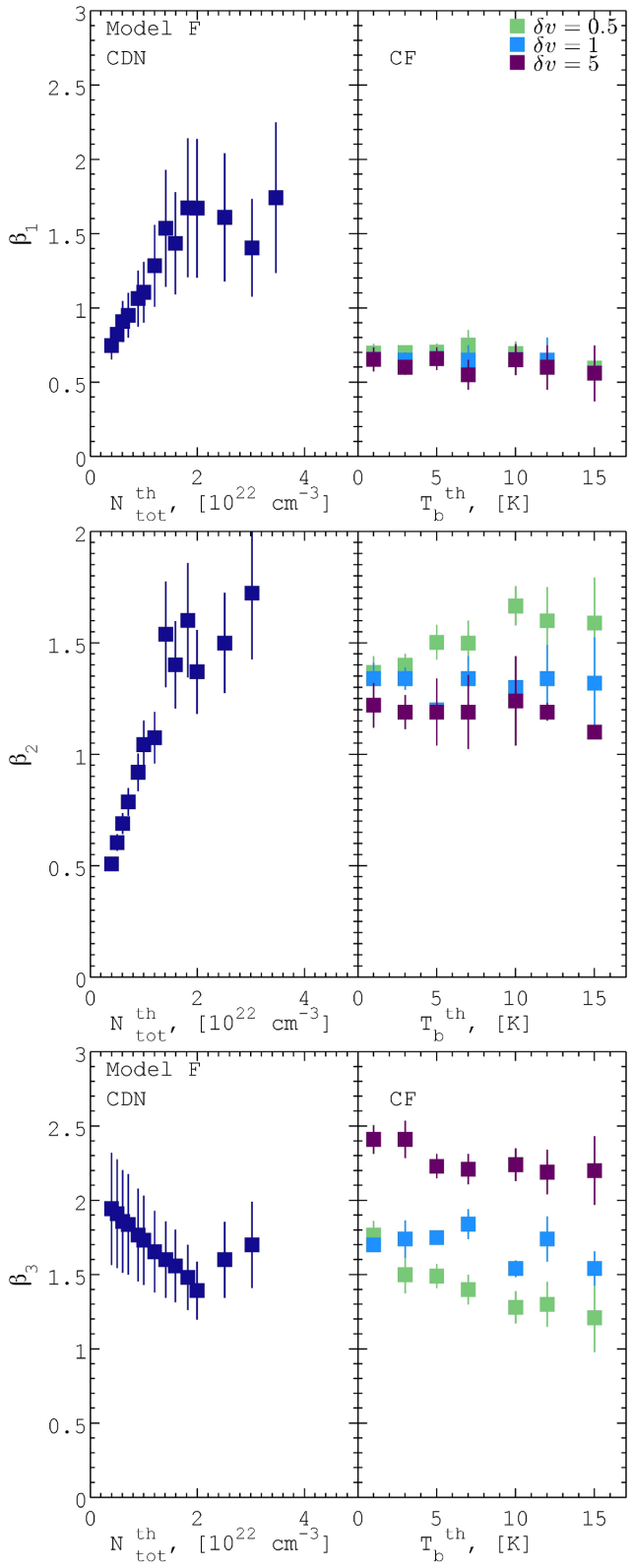

Figure 8. The power-law indices for the scaling relations, β_i, $i = 1, 2, 3$, as function of the total column density threshold $N_{\rm tot}^{\rm th}$ for clouds extracted using CDN approach (left panels). In the right panels the indices β_i are shown as a function of the brightness temperature $T_{\rm b}^{\rm th}$ for the cloud samples found in analysis of CO line spectra using the CF method for various spectral resolution δv.

clouds change dramatically in the case where the CDN method is used. Better agreement with the observational data can be found only with relatively low threshold values $\approx$0.5–1 $\times$ 10^{22} cm^{-2}.

In contrast, use of the CF method does not provide any significant variations of the scaling relation indices with threshold (see the right panels in Fig. 8). In this case, cloud populations vanish from capture of the intercloud medium, because this extraction method relates directly to regions with a high molecular fraction. This explains why the result remains robust relative to variation of the brightness temperature threshold value. The indices obtained using the CF criterion are close to the observed ones over a wide range of threshold values. Moreover, one cannot see a significant dependence on velocity resolution for the first scaling relation. For the other relations, the decrease of resolution leads to a systematic shift of the index values, so that the dependence on threshold value remains more or less flat.

5.6 Cloud mass spectra

The indices of the GMC scaling relations vary slightly for galaxies with different morphology, although both methods of cloud definition suffer from so-called environmental effects (see Figs 5, 6 and 7). In our case, such effects come from remarkable large-scale structures like spiral arms and a galactic bar.

To check the impact of the galactic environment on the cloud properties, we calculate the cumulative mass functions for three types of galaxy, i.e. the number of clouds N with masses $M_{\rm cl}$ greater than a reference mass $M'_{\rm cl}$:

$$N(M'_{\rm cl}) = N(M_{\rm cl} < M'_{\rm cl})\,. \tag{9}$$

The mass spectrum of molecular clouds is usually expressed as a power-law function (see e.g. Rosolowsky 2007; Gratier et al. 2012); however, a more accurate approach is based on the truncated power-law shape (Williams & McKee 1997; Colombo et al. 2014), which can be written in the form

$$N(M_{\rm cl} < M'_{\rm cl}) = N_0 \left[\left(\frac{M_{\rm cl}}{M'_{\rm cl}} \right)^{\gamma+1} - 1 \right], \tag{10}$$

where the index γ shows how the mass is distributed in the cloud population.

We compute fits of the cumulative mass distribution in the form (10) (Fig. 9). For all models considered, the slope of the mass distribution function γ (equation 10) is greater than -2, which means that large massive clouds dominate in the total GMC mass budget. One can see that clouds in CDN samples have a rather steeper mass distribution than for the CF sample. This demonstrates that most molecular mass tends to be concentrated in less massive clouds in the CF sample than in the CDN one. In other words, small clouds are more numerous in the CF sample. This is clearly seen from Fig. 4 and even from Fig. 9, if one mentions that the total masses of extracted clouds obtained using both methods are very close to each other. Such a conclusion is general for all three galaxy models (see Fig. 9).

A remarkable truncation of the mass distribution is seen for the CDN cloud samples in all models. This can be explained by the engaging of numerous structures above the column density threshold in the dense environment. This suggestion is confirmed by Fig. 9, where one can see that this effect is more clear in the galaxy with prominent spiral pattern and bar (model F) and weaker in the galaxy without structure (model B). Such significant truncation does not reflects the physical state of isolated molecular clouds, because the truncation is not detected for the CF sample of GMCs.

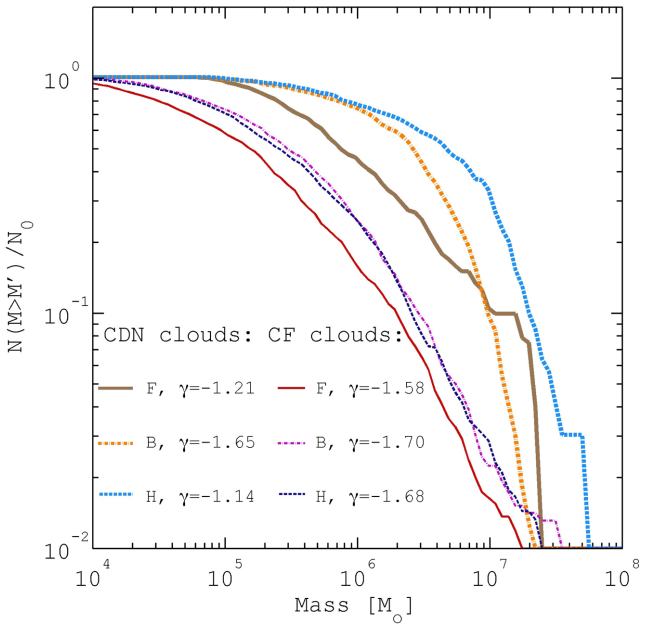

Figure 9. The mass spectrum of GMCs extracted using the CDN (top three lines) and CF (bottom three lines) methods in the models of galaxies (Table 1). The index γ for the mass spectrum in the form (10) is shown in the legend.

As was mentioned above (see Sections 5.1, 5.2 and 5.3), there are not strong variations of the scaling relation indices on galactic morphology for the same CD criterion. However, the impact of the galactic environment on GMC properties is clearly revealed and is seen in the mass distribution profiles in Fig. 9. The shapes of the distributions for CF samples are quite similar to each other: the γ values are in the range $[-1.70; -1.13]$, which once again shows the homogeneity of these cloud samples. This is especially remarkable for the galaxies without a large-scale pattern: models B and H. Note that for the CDN samples the distributions coincide for $M \lesssim 10^6$ M$_\odot$. The mass spectrum in model F differs systematically from the others. We suggest that stronger stellar feedback and compression of GMCs in spiral arms taken place in model F and affects the GMC mass distribution substantially. However, the conformity of the scaling relations (see Table 2) indicates that GMCs save their internal structure or the CD methods work in a similar way and, as a result, extracted structures (clouds) have rather close physical parameters. A similar influence of large-scale structures can be noticed in both numerical simulations of M83 (Fujimoto et al. 2014) and observations of M51 (Colombo et al. 2014). A more detailed discussion of such influence on statistical properties of clouds from the observational point of view can be found in Hughes et al. (2013).

6 CONCLUSIONS

In this article, we have presented a set of galactic-scale simulations of MW size galaxies of different morphological type: a galaxy without prominent structure, a spiral barred galaxy and a galaxy with flocculent structure. In our models we have taken into account star formation, stellar feedback, UV radiation transfer and non-equilibrium chemical kinetics for CO and H_2 molecules. Here we have focused on the statistical properties of molecular clouds obtained by two different extraction methods of gaseous structures. The first uses the total hydrogen column density threshold as a marker of the cloud border. The other cloud definition method is based on extraction from position–position–velocity (PPV) data cubes for the ^{12}CO (1–0) line. Using both methods, we have studied the empirical scaling relations known as Larson's laws: 'velocity dispersion–cloud size', 'luminosity–cloud size' and 'virial mass–luminosity' relations. Using our simulations, we have created position–position–velocity data cubes for several values of velocity resolution and have investigated how the physical parameters of clouds and the indices of the scaling relations depend on spectral resolution. Our results can be summarized as follows.

(i) The number of spatially resolved molecular clouds in the simulations depends slightly on galactic type and equals $\sim 10^3$; size, mass, luminosity and other physical properties of giant molecular clouds obtained in the simulations are close to those observed in our and nearby disc galaxies; note that the physical parameters of clouds depend on the cloud definition method (see Figs 3, 5, 6 and 7).

(ii) The diffuse (intercloud) gas can be caught using total column density as a threshold in the extraction of clouds; this can be especially significant in dense large-scale structures, e.g. within spiral arms or a bar; such diffuse gas has higher velocity dispersion and lower CO line brightness in comparison with other cloud material, so that using this method of extraction we cannot exclude overestimation of the 1D velocity dispersion due to projection effects, even at high total column density threshold $N_{\rm tot}^{\rm th}$ values.

(iii) Giant molecular clouds found using the CLUMPFIND (CF for shortness) algorithm have smaller sizes, masses and velocity dispersion than those extracted using total column density as a threshold. However, the distributions of the virial parameter for both extraction methods show similar behaviour (see Fig. 4).

(iv) Numerical models of galaxies with different morphology produce a substantial number of rather small GMCs ($R_{\rm cl} < 20$ pc), which are detectable by various methods considered in the article (see Fig. 4a). This is more clear for position–position–velocity analysis, where large clouds are split into smaller ones due to complex kinematics of gaseous flows. However, analysis of the mass distribution functions shows that the mass of the cloudy phase in galaxies simulated here is mostly concentrated in large massive clouds (see Fig. 9).

(v) Physical parameters of GMCs depend weakly on galactic structure: namely mass, size, luminosity and velocity dispersion are locked in the same ranges for models of galaxies without structure, with a prominent spiral pattern and with a flocculent pattern (see Figs 5, 6 and 7). Indeed, we do not see statistically sensible variations of the scaling relations in models of galaxies with different morphology for a given CD criterion (see Table 2); however, so-called environmental effects can be clearly seen in the distributions of cloud masses: the mass spectra are steeper in the galaxy with prominent structure (see Fig. 9).

Thus, we conclude that it is impossible to extract equivalent cloud populations by using the two different cloud extraction methods considered here: the first is based on total column density as threshold and the second utilizes PPV data analysis. Obviously, the comparison between observational and simulated properties of GMCs should be based on the same cloud extraction technique. The significant role of the cloud definition method and selection criteria (e.g. spectral resolution, threshold value, etc.) could correspond to the fact that the observable scaling relations for external galaxies might not completely reflect the real physical parameters of the ISM cold phase.

ACKNOWLEDGEMENTS

We thank our referee, Erik Rosolwski, kindly for thoughtful suggestions that greatly improved the quality of the article. We also thank Marco Lombardi for several stimulating discussions and for reading the early versions of the manuscript. The numerical simulations have been performed at the Research Computing Center (Moscow State University) under a Russian Science Foundation grant (14-22-00041) and Joint Supercomputer Center (Russian Academy of Sciences). This work was supported by RFBR grants (14-02-00604, 15-02-06204, 15-32-21062) and by a President of the RF grant (MK-4536.2015.2). SAK has been supported by a postdoctoral fellowship sponsored by the Italian MIUR. AMS has been supported by the Ministry of Education and Science of the Russian Federation within the framework of the research activities (project no. 3.1781.2014/K). This work was also supported by Act 211 Government of the Russian Federation, contract no 02.A03.21.0006. EOV is thankful to the Ministry of Education and Science of the Russian Federation (project 2663) and RFBR (projects 15-02-08293 and 15-52-45114). The thermochemical part was developed under support from the Russian Scientific Foundation (grant 14-50-00043).

REFERENCES

Allen R. J., Hogg D. E., Engelke P. D., 2015, AJ, 149, 123
Asplund M., Grevesse N., Sauval A. J., 2005, in Barnes T. G., III, Bash F. N., eds, ASP Conf. Ser. Vol. 336, Cosmic Abundance as Records of Stellar Evolution and Nucleosynthesis. Astron. Soc. Pac., San Francisco, p. 25
Bakes E. L. O., Tielens A. G. G. M., 1994, ApJ, 427, 822
Benincasa S. M., Tasker E. J., Pudritz R. E., Wadsley J., 2013, ApJ, 776, 23
Berry D. S., Reinhold K., Jenness T., Economou F., 2007, in Shaw R. A., Hill F., Bell D. J., eds, ASP Conf. Ser. Vol. 376, Astronomical Data Analysis Software and Systems XVI. Astron. Soc. Pac., San Francisco, p. 425
Bertoldi F., McKee C. F., 1992, ApJ, 395, 140
Bigiel F., Bolatto A. D., Leroy A. K., Blitz L., Walter F., Rosolowsky E. W., Lopez L. A., Plambeck R. L., 2010, ApJ, 725, 1159
Bolatto A. D., Leroy A. K., Rosolowsky E., Walter F., Blitz L., 2008, ApJ, 686, 948
Bolatto A. D., Wolfire M., Leroy A. K., 2013, ARA&A, 51, 207
Braun H., Schmidt W., Niemeyer J. C., Almgren A. S., 2014, MNRAS, 442, 3407
Caldú-Primo A., Schruba A., Walter F., Leroy A., Bolatto A. D., Vogel S., 2015, AJ, 149, 76
Cen R., 1992, ApJS, 78, 341
Colombo D. et al., 2014, ApJ, 784, 3
Combes F. et al., 2014, A&A, 565, A97
Dame T. M., Hartmann D., Thaddeus P., 2001, ApJ, 547, 792
Dickman R. L., 1975, ApJ, 202, 50
Dickman R. L., 1978, ApJS, 37, 407
Dobbs C. L., 2008, MNRAS, 391, 844
Dobbs C. L., Pringle J. E., 2013, MNRAS, 432, 653
Dobbs C. L., Bonnell I. A., Pringle J. E., 2006, MNRAS, 371, 1663
Dobbs C. L., Glover S. C. O., Clark P. C., Klessen R. S., 2008, MNRAS, 389, 1097
Dobbs C. L., Burkert A., Pringle J. E., 2011, MNRAS, 413, 2935
Donovan Meyer J. et al., 2013, ApJ, 772, 107
Draine B. T., Bertoldi F., 1996, ApJ, 468, 269
Engargiola G., Plambeck R. L., Rosolowsky E., Blitz L., 2003, ApJS, 149, 343
Feldmann R., Gnedin N. Y., Kravtsov A. V., 2012, ApJ, 758, 127
Fujimoto Y., Tasker E. J., Wakayama M., Habe A., 2014, MNRAS, 439, 936
Galli D., Palla F., 1998, A&A, 335, 403
Gil de Paz A. et al., 2007, ApJ, 173, 185
Glover S. C. O., Clark P. C., 2012, MNRAS, 421, 116
Glover S. C. O., Federrath C., Mac Low M.-M., Klessen R. S., 2010, MNRAS, 404, 2
Goldsmith P. F., Langer W. D., 1978, ApJ, 222, 881
Gratier P. et al., 2012, A&A, 542, A108
Heyer M., Krawczyk C., Duval J., Jackson J. M., 2009, ApJ, 699, 1092
Hindmarsh A. C., Brown P. N., Grant K. E., Lee S. L., Serban R., Shumaker D. E., Woodward C. S., 2005, ACM Trans. Math. Soft., 31, 363
Hollenbach D., McKee C. F., 1979, ApJS, 41, 555
Hollenbach D., McKee C. F., 1989, ApJ, 342, 306
Hopkins P. F., Quataert E., Murray N., 2012, MNRAS, 421, 3488
Hughes A. et al., 2013, ApJ, 779, 46
Khoperskov A. V., Zasov A. V., Tyurina N. V., 2003, Astron. Rep., 47, 357
Khoperskov S. A., Vasiliev E. O., Sobolev A. M., Khoperskov A. V., 2013, MNRAS, 428, 2311
Khoperskov S. A., Vasiliev E. O., Khoperskov A. V., Lubimov V. N., 2014, J. Phys. Conf. Ser., 510, 012011
Koda et al., 2009, ApJ, 700, L132
Kraljic K., Renaud F., Bournaud F., Combes F., Elmegreen B., Emsellem E., Teyssier R., 2014, ApJ, 784, 112
Kritsuk A. G., Lee C. T., Norman M. L., 2013, MNRAS, 436, 3247
Larson R. B., 1981, MNRAS, 194, 809
Leitherer C. et al., 1999, ApJS, 123, 3
Leroy A. K. et al., 2009, AJ, 137, 4670
Meidt S. E. et al., 2015, ApJ, 806, 72
Nelson R. P., Langer W. D., 1999, ApJ, 524, 923
Omukai K., 2000, ApJ, 534, 809
Renaud F. et al., 2013, MNRAS, 436, 1836
Roman-Duval J., Jackson J. M., Heyer M., Johnson A., Rathborne J., Shah R., Simon R., 2009, ApJ, 699, 1153
Roman-Duval J., Jackson J. M., Heyer M., Rathborne J., Simon R., 2010, ApJ, 723, 492
Romeo A. B., Wiegert J., 2011, MNRAS, 416, 1191
Rosolowsky E., 2007, ApJ, 654, 240
Rosolowsky E., Leroy A., 2006, PASP, 118, 590
Schinnerer E. et al., 2013, ApJ, 779, 42
Scoville N. Z., Solomon P. M., Sanders D. B., 1979, in Burton W. B., ed., IAU Symp. Vol. 84, The Large-Scale Characteristics of the Galaxy. Reidel, Dordrecht, p. 277
Shetty R., Ostriker E. C., 2008, ApJ, 684, 978
Solomon P. M., Rivolo A. R., Barrett J., Yahil A., 1987, ApJ, 319, 730
Tan B.-K. et. al., 2013, MNRAS, 436, 921
Tasker E. J., 2011, ApJ, 730, 11
Tasker E. J., Tan J. C., 2009, ApJ, 700, 358
Visser R., van Dishoeck E. F., Black J. H., 2009, A&A, 503, 323
Williams J. P., McKee C. F., 1997, ApJ, 476, 166
Williams J. P., de Geus E. J., Blitz L., 1994, ApJ, 428, 693
Wolfire M. G., McKee C. F., Hollenbach D., Tielens A. G. G. M., 2003, ApJ, 587, 278
Zasov A., Kasparova A., 2014, Astron. Space Sci., 353, 595

This paper has been typeset from a TEX/LATEX file prepared by the author.